Processing and Application of Ceramics 18 [1] (2024) 109–116
https://doi.org/10.2298/PAC2401109F

Preparation and properties of novel tungstate $SrLa_6W_{10}O_{40}$: Eu^{3+} phosphors

Guo Feng[1,*], Xiaolong Huang[1], Feng Jiang[1], Qing Yang[1], Wenwei Jin[1], Chuan Shao[2], Jianmin Liu[1], Wang Dahai[3], Liang Jian[1]

[1]*Department of Material Science and Engineering, Jingdezhen Ceramic Institute, Jingdezhen 333000, China*
[2]*Market Supervision and Management of Jingdezhen City Comprehensive Inspection and Testing Center, Jingdezhen 333000, China*
[3]*Jingdezhen Red Leaf Ceramics Co. Ltd, Jingdezhen 333000, China*

Received 4 November 2023; Received in revised form 7 March 2024; Accepted 22 March 2024

Abstract

Novel tungstate $SrLa_{6-x}W_{10}O_{40}$: xEu^{3+} (x = 0, 0.03, 0.06, 0.09, 0.12, 0.15, 0.18, 0.21) red phosphors were prepared by solid state method at 1150 °C by using $SrCO_3$, La_2O_3, WO_3 and Eu_2O_3 as raw materials. The powders were agglomerated with particles having mostly spheroidal morphology, mean particle size D_{50} = 12.8 μm and narrow particle size distribution. With the increase of doping amount x, there is no significant difference in the diffraction peak position of the phosphor, but the cell volume of $SrLa_6W_{10}O_{40}$ slowly decreases. The relative strength of diffraction peaks decreases gradually and the half-peak width widens gradually, indicating that the inclusion of Eu^{3+} ions affects the crystallization of the $SrLa_6W_{10}O_{40}$ matrix. Excitation and emission spectra of the prepared samples were obtained. The optimal doping content has the $SrLa_{5.85}W_{10}O_4$: $0.15Eu^{3+}$ phosphor and is characterised with the colour coordinate of (0.652, 0.348), which is closer to the red standard colour (0.67, 0.33) than the near-ultraviolet red phosphor Y_2O_2S: Eu^{3+} (0.622, 0.351) used for commercial LED.

Keywords: *Eu-doped $SrLa_6W_{10}O_{40}$, phosphor, powder, structure, luminescence properties*

I. Introduction

Tungstate is one of the most classic inorganic luminescent materials. As early as 1896, Pupin discovered that $CaWO_4$ could be applied for X-ray luminescence, and it was first used as an X-ray luminescence material in 1906 [1]. In recent years, the application of tungstate activated by rare earth ion Eu^{3+} in white LED is also significant [2–4]. However, there are no reports on the preparation of phosphors with rare earth ion doping or transition metal ion doping of $SrLa_6W_{10}O_4$. Therefore, $SrLa_6W_{10}O_{40}$: Eu^{3+} phosphor was studied in this paper.

LED is a solid-state light source that has the characteristics of long lifespan, low energy consumption, energy conservation and low-carbon, no ultraviolet radiation and no mercury pollution. At present, it has been widely used in various fields such as indicator lights, displays, lighting, communication, etc. [5–7]. LED is a new and important light source in the 21st century. Among them phosphor conversion (PC) white LED has received much attention. At present, the main problems with white light LEDs are: i) too high costs, especially the cost of high brightness LEDs [8], ii) very low luminous efficiency of LED [9] and iii) lack of high-performance fluorescent powders. Su *et al.* [10] pointed out that the most prominent problem with the white LED scheme combining InGaN blue chip with YAG: Ce yellow fluorescent powder is that the white LED colour rendering index is only 60–70, and it is difficult to exceed 75. Generally, indoor lighting requires a colour rendering index of the light source greater than 80, and the white light scheme combining blue LED and yellow powder mentioned above cannot be achieved separately. The main reason for this result is that the proportion of red light in YAG: Ce fluorescent powder and the intensity are low. In YAG: Ce fluorescent powder, the red light spectral energy only accounts for 8% to 15% of the total spectral energy, which is much lower than

*Corresponding author: tel: +86 798 8499328
e-mail: *fengguo@jci.edu.cn*

the proportion of yellow green light. Therefore, in order to improve the colour rendering index of packaged LED light sources and obtain products with appropriate colour temperature, a certain amount of red fluorescent powder must be added to YAG: Ce fluorescent powder during packaging. Currently, almost all low colour temperature white LED products on the market are manufactured using this method. However, efficient red fluorescent powder has become a bottleneck in the development of white LED [11], and currently, in the scheme of adding RGB fluorescent powder to ultraviolet chips, the efficiency of red, green and blue fluorescent powders has been greatly improved, but the efficiency of red fluorescent powder is the lowest [12]. The development of new red fluorescent powders is a key issue in achieving high-performance light conversion white LED [12,13], which also makes the development of high-efficiency red fluorescent powders for LED a current research hotspot.

The reported fluorescent powder preparation methods include: solid state method [14–16], sol-gel method [17–19], precipitation method [20,21], spray drying method [22,23], ultrasonic spray pyrolysis method [24,25], hydrothermal method [26,27], etc. The wet chemical method used to prepare fluorescent powder might have relatively good powder morphology, and the relative brightness may be similar to that of samples prepared by high-temperature solid state method. In some systems, the relative brightness can even be comparable to that of samples prepared by high-temperature solid state method (in general, the relative brightness of fluorescent powder prepared by wet chemical method is only 70% to 80% of that prepared by high-temperature solid state method. However, the above methods have the drawbacks of low production or high equipment requirements, which are not conducive to the practical application of fluorescent powders with important practical significance. In addition, wet chemical methods inevitably result in loss of raw materials during the preparation process, leading to significant errors in experimental reproducibility. Therefore, in this article we adopted the solid state method to prepare samples.

II. Experimental

The starting materials $SrCO_3$ (Shanghai Aladdin Co. Ltd.), La_2O_3 (Shanghai Aladdin Co. Ltd.), WO_3 (Sinopharm Chemical Reagent Co. Ltd.) and Eu_2O_3 (Sinopharm Chemical Reagent Co. Ltd.) were weighted according to the nominal compositions $SrLa_{6-x}W_{10}O_{40}$: xEu^{3+} (x = 0, 0.03, 0.06, 0.09, 0.12, 0.15, 0.18, 0.21). Then they were blended in agate mortar and calcined in an alumina crucible at 1150 °C for 2 h in air to complete conventional solid state reactions.

Phase composition of the $SrLa_6W_{10}O_{40}$: Eu^{3+} phosphors was identified by recording the powder X-ray diffraction (XRD) patterns using X'pert PRO X-ray diffractometer with Cu Kα_1 radiation (λ = 1.54056 Å). Microstructure of the samples was observed by field-emission scanning electron microscopy (FE-SEM, SU-8010, JEOL, Japan). The particle size and distribution of the powders were characterized by laser particle size analyser (Mastersizer 3000, Malvern, UK). Excitation and emission spectra were measured by using Hitachi F-4500 spectrofluorometer equipped with a 60 W Xenon lamp as excitation source. The chromaticity data were taken by using the PMS-50 spectra analysis system. All of the measurements were performed at room temperature.

III. Results and discussion

3.1. Phase composition

Figure 1 shows XRD patterns of the prepared powders with the nominal compositions $SrLa_{6-x}W_{10}O_{40}$: xEu^{3+} where x = 0, 0.03, 0.06, 0.09, 0.12, 0.15, 0.18 and 0.21. It can be seen from Fig. 1 that the diffraction peaks of all samples containing Eu^{3+} are identical to those of the $SrLa_6W_{10}O_{40}$ (PDF card No. 29-1463) in the range of $10° \leq 2\theta \leq 60°$. No secondary phase diffraction peaks were detected. It is worth noting that the relative intensity of the XRD peaks becomes lower and the half-peak width gradually becomes wider with the increase of Eu^{3+} ions doping under the same preparation and testing conditions. The results indicated that the incorporation of Eu^{3+} ions hindered the crystallization of $SrLa_6W_{10}O_{40}$.

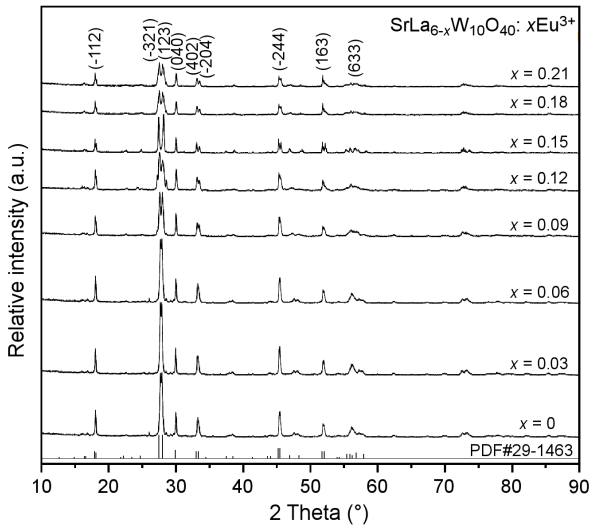

Figure 1. XRD patterns of $SrLa_{6-x}W_{10}O_{40}$: xEu^{3+}

In order to facilitate clear comparison, XRD patterns of the $SrLa_6W_{10}O_{40}$ and $SrLa_{5.85}W_{10}O_{40}$: 0.15Eu^{3+} samples are shown in Fig. 2. The XRD patterns of both phosphor samples are similar to that of the $SrLa_6W_{10}O_{40}$ phase (PDF card No. 29-1463) regarding to peak position and relative intensity. No other diffraction peaks of any impurity phase were detected in the XRD patterns. In addition, there is no obvious peak position shift in the XRD patterns of $SrLa_6W_{10}O_{40}$ and $SrLa_{5.85}W_{10}O_{40}$: 0.15Eu^{3+} samples. These results indicated that the addition of Eu^{3+} ions did not change the

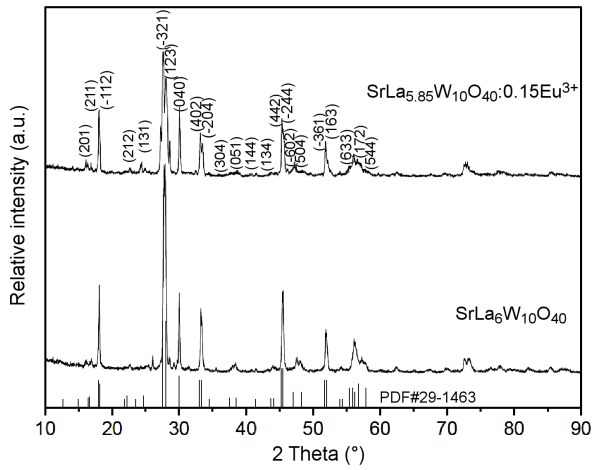

Figure 2. XRD patterns of $SrLa_6W_{10}O_{40}$ and $SrLa_{5.85}W_{10}O_{40}$: $0.15Eu^{3+}$ powders

Table 1. Unit cell parameters and unit cell volume (V) of $SrLa_{6-x}W_{10}O_{40}$: xEu^{3+}

Doping content, x	a [Å]	b [Å]	c [Å]	V [Å^3]
0	12.2019	11.8814	11.9513	1732.56
0.03	12.0794	11.9081	12.0274	1730.06
0.06	12.1653	11.8875	11.9506	1728.15
0.09	12.1884	11.9083	11.8947	1726.43
0.15	12.1849	11.8802	11.9023	1722.88
0.18	12.2004	11.8975	11.8649	1722.16
0.21	12.1882	11.8957	11.8759	1721.81

crystal structure of $SrLa_6W_{10}O_{40}$, resulting in the formation of single phase material. The cell parameters and cell volume of the $SrLa_{6-x}W_{10}O_{40}$: xEu^{3+} (x = 0, 0.03, 0.06, 0.09, 0.12, 0.15, 0.18, 0.21) samples are given in Table 1. In the investigated compositional range, cell volume of the sample decreases slowly with the increase of Eu^{3+} doping amount. This indicates that Eu^{3+} ions are incorporated into the $SrLa_6W_{10}O_{40}$ lattice. The reasons why the $SrLa_6W_{10}O_{40}$ crystal structure is not changed with addition of Eu^{3+} ions are the valence state of Eu^{3+} and La^{3+} ions and similar radius of Eu^{3+} and La^{2+} ions for the same coordination number [28] (when the coordination number CN = 8, the radii of Eu^{3+} and La^{3+} ions are 0.107 nm [29] and 0.116 nm [28], respectively). However, it can be concluded that the Eu^{3+} doping affects the crystallization of $SrLa_6W_{10}O_{40}$, since at higher Eu^{3+} ion doping the diffraction peak intensity and the half-peak width of each diffraction peak gradually increases.

In order to further investigate the influence of Eu^{3+} ion doping on the crystal structure of $SrLa_6W_{10}O_{40}$, the undoped $SrLa_6W_{10}O_{40}$ sample and the $SrLa_{5.85}W_{10}O_{40}$: $0.15Eu^{3+}$ with the best luminescence performance were mixed according to mass ratio 1:1 and analysed by XRD (Fig. 3). It can be seen from Fig. 3a that the diffraction peak corresponding to each crystal plane of the powder mixture has a relatively obvious fork peak, showing a small peak next to the main peak. In order to make this fork peak more obvious, the diffraction peak corresponding to the (400) crystal plane (2θ = 29.970°) in the mixed powder is magnified (Fig. 3b). This confirmed that the XRD peak corresponding to the crystal plane (400) is fork peak (Fig. 3b), and the positions of two peaks are 2θ = 30.037° and 30.122°, respectively. This is a manifestation of the influence of doping ions entering the lattice on the matrix lattice. It is worth noting that the relative strength of the fork peak at higher angle 2θ = 30.122° is weaker than that at lower angle 2θ = 30.037°. It corresponds to the gradual weakening of the relative intensity of the XRD peaks with the increase of Eu^{3+} ion doping (under the same preparation and test conditions). These phenomena confirm that Eu^{3+} ions have doped into the matrix lattice.

3.2. Morphology analysis

Figure 4 shows SEM micrographs of the $SrLa_{5.85}W_{10}O_{40}$: $0.15Eu^{3+}$ phosphor sample heated at 1150 °C for 2 h. It can be seen from Fig. 4 that the sample consists of agglomerated particles which are partially sintered during the heat treatment process. The particles do not show obvious consistent shape (some

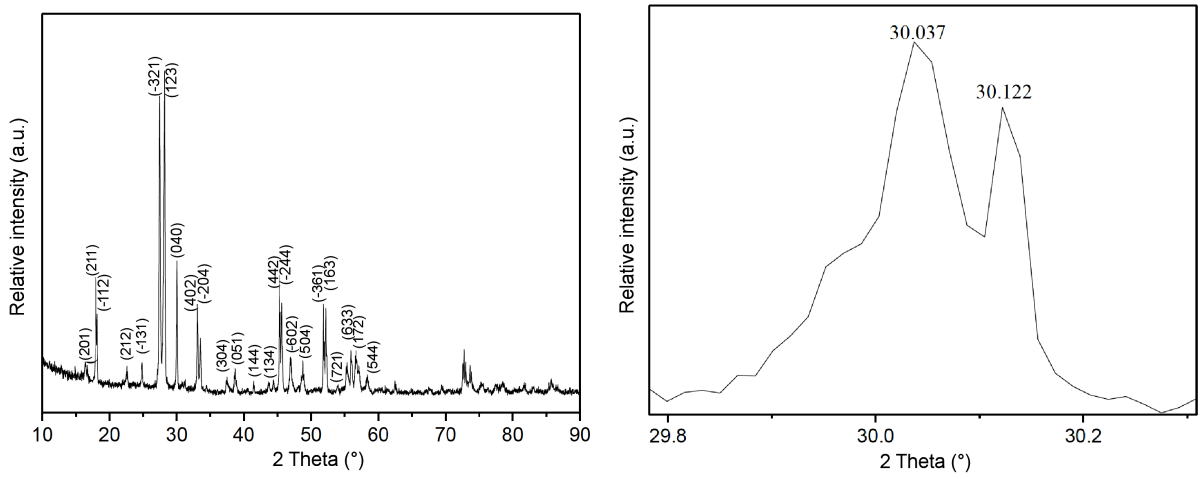

Figure 3. XRD pattern of $SrLa_6W_{10}O_{40}$ and $SrLa_{5.85}W_{10}O_{40}$: $0.15Eu^{3+}$ mixed powder (a) and enlarged XRD pattern (b)

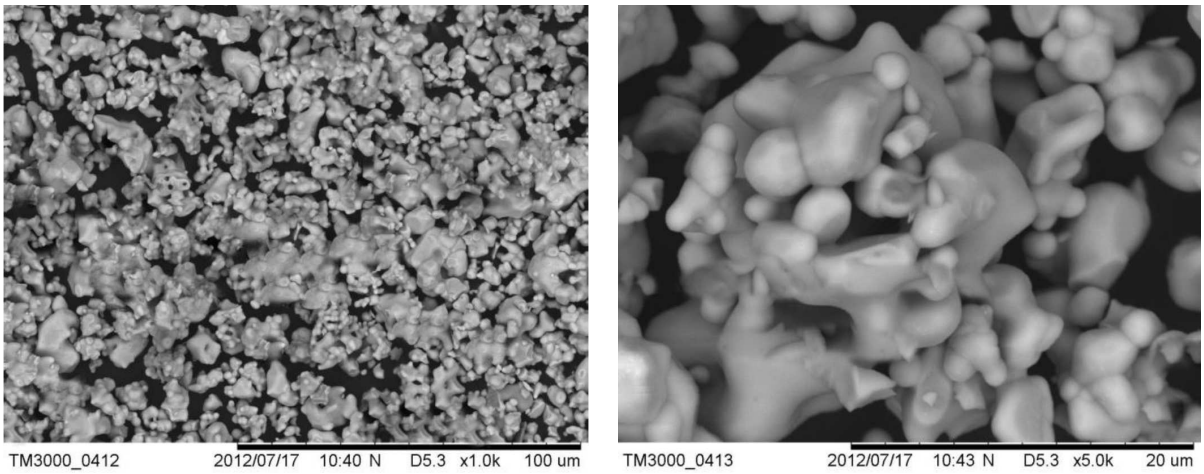

Figure 4. SEM photographs of the $SrLa_{5.85}W_{10}O_{40}$: 0.15Eu^{3+} phosphor

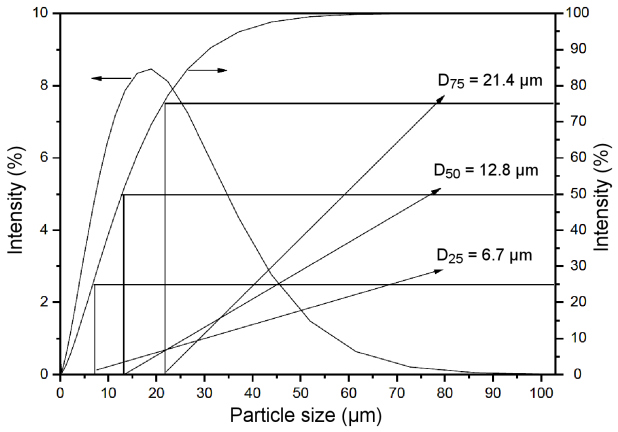

Figure 5. Particle size distribution of $SrLa_{5.85}W_{10}O_{40}$: 0.15Eu^{3+} phosphor

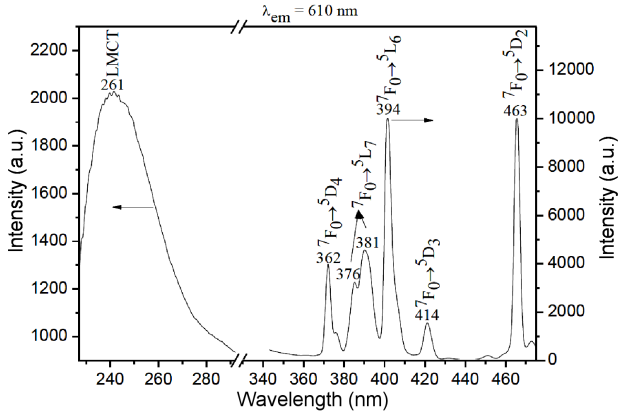

Figure 6. Excitation spectrum of $SrLa_{5.85}W_{10}O_{40}$: 0.15Eu^{3+} phosphor

particles are spherical) and the particle size ranged from one to dozens of μm with the average particle size of about 13 μm. The grain edges and surfaces are clear, indicating that the sample has good crystallization and good grain development, which corresponds to the XRD results showing high diffraction peak intensity and narrow half-peak width.

Figure 5 shows the laser particle size test results of $SrLa_{5.85}W_{10}O_{40}$: 0.15Eu^{3+} phosphor. The D_{50} of the $SrLa_{6-x}W_{10}O_{40}$: xEu^{3+} phosphor sample is 12.8 μm (Fig. 5), which is similar to the average particle size obtained by SEM. The particle size distribution, evaluated by $(D_{75} - D_{25})/(D_{25} + D_{75})$, where D_{25} = 6.74 μm and D_{75} = 21.4 μm, is relatively narrow since the corresponding ratio is 0.52.

3.3. Optical properties

Excitation spectra

Figure 6 shows the excitation spectrum (measured with light having wavelength of λ_{em} = 610 nm) of the $SrLa_{5.85}W_{10}O_{40}$: 0.15Eu^{3+} phosphor sample, showing an absorption band in the range of 210–280 nm with maximum at 261 nm. This absorption band contains the following three components - ligand-to-metal charge-transfer (LMCT) formed by electron transfer from: (1) O^{2-} to Eu^{3+}, (2) O^{2-} to W^{6+} and (3) from tungstate to Eu^{3+} [30]. This also indicates that Eu^{3+} ions have been doped into the $SrLa_6W_{10}O_{40}$ matrix lattice.

The excitation spectra also have 5 peaks at around 362, 376, 381, 394, 414 and 463 nm. The peak at 350 nm belongs to the *f-f* (i.e., the intrinsic excitation peak of Eu^{3+} ion) excitation peak of Eu^{3+}. The two strong peaks are located at 394 and 463 nm, corresponding to the $^7F_0 \rightarrow {}^5L_6$ and $^7F_0 \rightarrow {}^5D_2$ transitions of Eu^{3+}, respectively. The excitation peak at 394 nm is strong and matches well with the emission wavelength of the near-ultraviolet region, indicating that the sample is an ideal phosphor for near ultraviolet LED. The excitation peak at 463 nm matches the emission wavelength of the blue region, indicating that the sample is also an ideal phosphor for the blue light LED. In addition, the excitation peak at 362 nm is attributed to the $^7F_0 \rightarrow {}^5D_4$ [31] level transition of Eu^{3+} ion, and the excitation peaks at 376 and 381 nm are formed by the $^7F_0 \rightarrow {}^5L_7$ level transition of Eu^{3+} ion [32,33]. The excitation peak at 414 nm is caused by the $^7F_0 \rightarrow {}^5D_3$ transition of Eu^{3+} ion [34]. In $SrLa_6W_{10}O_{40}$ matrix, the splitting of Eu_3^+ by $^7F_0 \rightarrow {}^5L_7$ level transition indicates that Eu^{3+} is in a distorted state in the matrix [35].

Emission spectra

Emission spectra of the $SrLa_{5.85}W_{10}O_{40}$: $0.15Eu^{3+}$ sample (excitation wavelengths were λ_{ex} = 254, 395 and 465 nm) are shown in Fig. 7. The emission spectra are basically consistent in terms of the peak position and shape of the emission peak, and the difference lies in the relative intensity of the peak. The relative intensity of the excitation peak at 254 nm is much lower than that of the peaks at 395 and 465 nm (which have similar relative intensities).

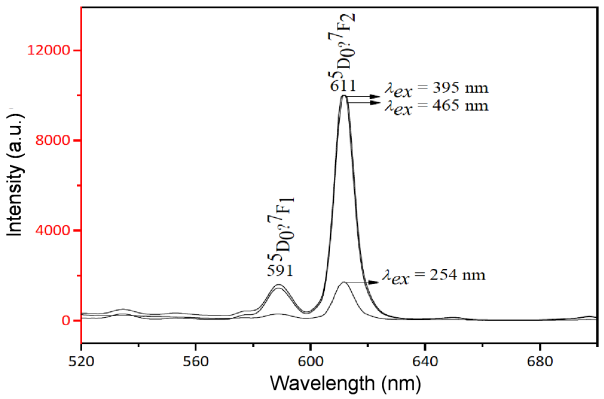

Figure 7. Emission spectra of $SrLa_{5.85}W_{10}O_{40}$: $0.15Eu^{3+}$ phosphor

The excitation peaks at 591 and 611 nm are attributed to the $^5D_0 \rightarrow {}^7F_1$ and $^5D_0 \rightarrow {}^7F_2$ level transitions of Eu^{3+} ion, respectively. In the $SrLa_6W_{10}O_{40}$ matrix, the $^5D_0 \rightarrow {}^7F_2$ level transition belonging to the electric dipole transition is stronger than the $^5D_0 \rightarrow {}^7F_1$ level transition belonging to the magnetic dipole transition. The electric dipole transition is caused by Eu^{3+} occupying the non-central symmetric sites in the matrix lattice and breaking the parity selection rule [36]. The strength of the transition depends on the symmetry of the lattice environment. The stronger the symmetry of the lattice environment, the weaker the strength is. The orange light emission peak at 591 nm is attributed to the $^5D_0 \rightarrow {}^7F_1$ magnetic dipole transition of Eu^{3+}, which is insensitive to the symmetry of the lattice environment [32]. The change of intensity ratio of red light emission to orange light emission of different samples (red to orange ratio) will quantitatively reflect the change of central symmetry of the lattice environment around Eu^{3+} ion. The higher the ratio, the lower the symmetry is. The emission intensity of red light at 611 nm is higher than that of orange light at 595 nm for the $SrLa_{5.85}W_{10}O_{40}$: $0.15Eu^{3+}$ phosphor, indicating that Eu^{3+} occupies the non-centrosymmetric site of the matrix lattice. High intensity $^5D_0 \rightarrow {}^7F_2$ red emission [37] is conducive to obtaining higher red colour purity. To sum up, the energy level transition diagram at λ_{ex} = 254 nm (this wavelength is chosen to draw the charge migration band) is shown in Fig. 8.

To further prove that the spectra above are indeed formed by doping Eu^{3+} ions into the $SrLa_6W_{10}O_{40}$ lattice, spectra of the sample with x = 0.15 without heat treatment were tested. Whether the excitation spectra are measured at λ_{em} = 610 nm or the emission spectra are measured at λ_{ex} = 254, 395 and 465 nm, there is no obvious excitation peak or emission peak. This further proves, to a certain extent, that Eu^{3+} ions have been doped into the $SrLa_6W_{10}O_{40}$ matrix lattice after heat treatment.

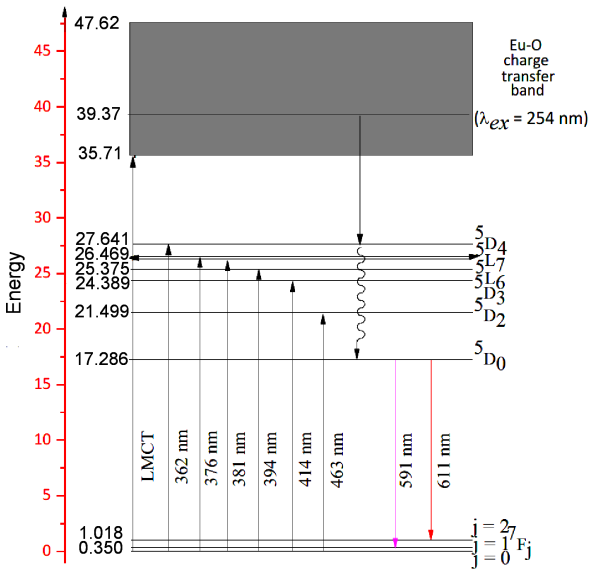

Figure 8. Energy level diagram of $SrLa_{5.85}W_{10}O_{40}$: $0.15Eu^{3+}$ phosphor exited at λ_{ex} = 254 nm

In general, rare earth ions form luminous centres in luminous materials, and the luminous intensity of materials is closely related to the doping amount of activated ions, namely the number of luminous centres [38]. Thus, the emission spectra of all investigated samples ($SrLa_{6-x}W_{10}O_{40}$: xEu^{3+} where x = 0, 0.03, 0.06, 0.09, 0.12, 0.15, 0.18 and 0.21) were measured for excitation wavelength of λ_{ex} = 395 nm (Fig. 9). It can be seen from Fig. 9 that under the excitation of 395 nm wavelength, when the Eu^{3+} doping amount is $x \leq 0.15$, the *f-f* emission intensity of Eu^{3+} in the emission spectrum gradually increases with the increase of the doping amount of rare earth ions. However, this trend changes when the doping amount x of Eu^{3+} is higher than 0.15, and the emission peak intensity decreases with the increase of doping amount. Therefore, Eu^{3+} doping amount x = 0.15 has the strongest fluorescence emission. For $x \leq 0.15$, the number of Eu^{3+} luminescent centres increases gradually with the increase of the doping amount of Eu^{3+}, and the distance between the luminescent Eu^{3+} centres becomes shorter, thus improving the luminescence intensity. However, when the doping amount of Eu^{3+} exceeds a certain value, non-radiative energy transfer between activator ions will occur, resulting in concentration quenching effect, which reduces the luminous intensity and luminous efficiency. Thus, when the doping amount of Eu^{3+} exceeds x = 0.15, the distance between Eu^{3+} becomes even closer, which makes the non-radiative energy transfer to dominate. There-

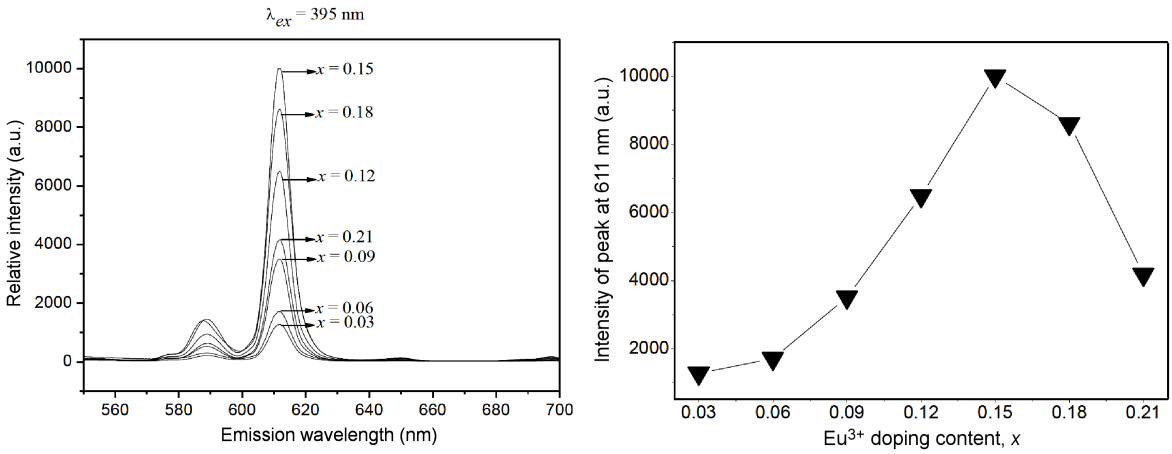

Figure 9. Emission spectra of phosphors with different Eu^{3+}-doping contents x (a) and intensities of the emission peak at 611 nm for different Eu^{3+}-doping contents (b)

fore, the fluorescence intensity decreases with the increase of the concentration of Eu^{3+} and the optimal doping amount in the $SrLa_{6-x}W_{10}O_{40}$: xEu^{3+} phosphor is x = 0.15.

The critical concentration of Eu^{3+} in $SrLa_6W_{10}O_{40}$ cell (χ_C) was calculated by the formula of critical distance R_{Eu-Eu}:

$$R_{Eu-Eu} = 2\left(\frac{3V}{4\pi \cdot \chi_C \cdot N}\right)^{1/3} \quad (1)$$

where V is the volume of the original cell and N is the number of matrix cations in the original cell. Since the cell volume of the $SrLa_{5.85}W_{10}O_{40}$: $0.15Eu^{3+}$ phosphor is 1.72288 nm^3 (Table 1) and the critical distance of Eu^{3+} in the $Srla_6W_{10}O_{40}$ cell is about 2.22 nm, critical quenching concentration was calculated to be 0.025.

Colour coordinate

Table 2 lists the colour coordinate values of samples with different doping amounts of Eu^{3+} ions. Difference of colour coordinate values for the samples with different Eu^{3+} ion doping contents is small, indicating that the sample has good chrominance stability [39]. The colour coordinates of the $SrLa_{5.85}W_{10}O_{40}$: $0.15Eu^{3+}$ phosphor are (0.652, 0.348) which is closer to the standard colour coordinate of red (0.67, 0.33) than that of Y_2O_2S: Eu^{3+} (0.622, 0.351) [40,41]. This indicates that $SrLa_{5.85}W_{10}O_{40}$: $0.15Eu^{3+}$ phosphor has very high colour purity. Therefore, the phosphor of tungstate system can be used as the red phosphor in white LED system with three primary colours in near ultraviolet chip. It can also be used as a complementary phosphor to make up for the deficiency of red light components in the commercialized InGaN blue chip plus YAG: Ce yellow phosphor white LED system and improve its colour rendering.

Table 2. Chromaticity coordinate values of $SrLa_{6-x}W_{10}O_{40}$: xEu^{3+} phosphors

Sample	x	y
$SrLa_{5.97}W_{10}O_{40}$: $0.03Eu^{3+}$	0.651	0.349
$SrLa_{5.95}W_{10}O_{40}$: $0.06Eu^{3+}$	0.651	0.348
$SrLa_{5.91}W_{10}O_{40}$: $0.09Eu^{3+}$	0.652	0.348
$SrLa_{5.88}W_{10}O_{40}$: $0.12Eu^{3+}$	0.652	0.348
$SrLa_{5.85}W_{10}O_{40}$: $0.15Eu^{3+}$	0.652	0.348
$SrLa_{5.82}W_{10}O_{40}$: $0.18Eu^{3+}$	0.652	0.348
$SrLa_{5.79}W_{10}O_{40}$: $0.21Eu^{3+}$	0.650	0.349

IV. Conclusions

Novel tungstate $SrLa_{6-x}W_{10}O_{40}$: xEu^{3+} (x = 0, 0.03, 0.06, 0.09, 0.12, 0.15, 0.18, 0.21) red phosphor powders were prepared by solid state method at 1150 °C for 2 h by using $SrCO_3$, La_2O_3, WO_3 and Eu_2O_3 as raw materials. The powders were agglomerated with particles having mostly spheroidal morphology, mean particle size D_{50} = 12.8 μm and narrow particle size distribution. XRD analyses confirmed that Eu^{3+} ions were incorporated in the tungstate lattice and there were no diffraction peaks of any impurity phase. With the increase of Eu^{3+} doping amount there was no significant difference in the diffraction peak position of the phosphor, but the cell volume of $SrLa_6W_{10}O_{40}$ slowly decreased.

The spectral analyses confirmed that the optimal doping amount in the $SrLa_{6-x}W_{10}O_{40}$: xEu^{3+} phosphor is x = 0.15. The excitation spectrum of $SrLa_{5.85}W_{10}O_{40}$: $0.15Eu^{3+}$ phosphor has an absorption band in the range of 210–340 nm with maximum at 280 nm. The main peak of its emission spectrum is 611 nm, which is the red emission generated by the $^5D_0 \rightarrow {}^7F_2$ level transition of Eu^{3+}. Therefore, the obtained tungstate can be used as the red phosphor of white LED system with three primary colours in near ultraviolet chip. The $SrLa_{5.85}W_{10}O_{40}$: $0.15Eu^{3+}$ powder has excellent luminous intensity and luminous efficiency. The quenching concentration is 0.025 and the critical distance of Eu^{3+} in $SrLa_6W_{10}O_{40}$ matrix is 2.22 nm.

Acknowledgements: This work was supported by

the National Natural Science Foundation of China [grant numbers 52072162, 51962014]; Jiangxi Provincial Natural Science Foundation [grant numbers 20202ACBL214008, 20192BBEL50022, 2020ZDI03004, 20232ACB204012]; the Jingdezhen Science and Technology plan project (2021ZDGG001, 20202GYZD013-09, 20202GYZD013-14); the Science Foundation of Jiangxi Provincial Department of Education (GJJ201318, GJJ201324, GJJ201345).

References

1. G. Blasse, "Classical phosphors: A Pandora's box", *J. Lumin*., **72** [74] (1997) 129–134.
2. G. Blasse, G.J. Dirksen, "On the luminescence of rare-earth activated bismuth tungstates", *J. Solid. State. Chem*., **42** [2] (1982) 163–169.
3. L.Y. He, X.Q. Li, "Synthesis and luminescence properties of $Sr_2ZnSi_2O_7$:Eu^{3+} at low temperature", *Chin. J. Lumin*., **35** [11] (2014) 1306–1310.
4. G. Blasse, G.J. Dirksen, "Luminescence and energy transfer in bismuth tungstate $Bi_2W_2O_9$", *Phys. Status. Solidi A*, **57** [1] (1980) 229–233.
5. N. Watch, "Resources: the LED grows up", *Science*, **296** [5568] (2002) 623.
6. J.L. Bu, Z.Y. Jiang, S.H. Jiao, "Irradiation damage of electron-beam on high-power AlInGaP red LED", *Adv. Mater*., **415** [417] (2012) 1297–1301.
7. E.F. Schubert, *Light-Emitting Diodes*, New York, Rensselaer Polytechnic Institute Press, 2006.
8. M.G. Craford, "LEDs challenge the incandescent", *IEEE Circuits Devices Magaz*., **8** [5] (1992) 24–29.
9. R.V. Steele, "High-brightness LED market overview", *Proceed. SPIE*, **4445** [12] (2001) 1–4.
10. C.F. Guo, D.X. Huang, Q. Su, "Methods to improve the fluorescence intensity of CaS: Eu^{2+} red-emitting phosphor for white LED", *Mater. Sci. Eng. B*, **130** (2006) 189–193.
11. X.H. He, J. Zhou, N. Lian, M.Y. Guan, "Dependence of photoluminescence performance on composition of novel red-emitting phosphors for white LEDs application", *Bull. Chinese Ceram. Soc*., **28** [4] (2009) 741–750.
12. M.R. Krames, O.B. Shchekin, R. Mueller-Mach, G.O. Mueller, L. Zhou, G. Harbers, M. George Craford, "Status and future of high-power light-emitting diodes for solid-state lighting", *J. Disp. Technol*., **3** [2] (2007) 160–175.
13. Q.Q. Hou, P.X. Zhang, M.F. Zhang, Z.W. Lu, X.Z. Ren, "Development of the research on high-power WLEDs", *Adv. Mater. Res*., **158** [3] (2010) 42–51.
14. V.D. Luong, W. Zhang, H.-R. Lee, "Synthesis of $Sr_2Si_5N_8$: Eu^{2+} phosphor for enhanced red emission", *Adv. Mater. Res*., **235** [2705] (2011) 2705–2709.
15. G. Feng., W.H. Jiang, Y.B. Chen, R. Zeng, "A novel red phosphor $NaLa_4(SiO_4)_3F$: Eu^{3+}", *Mater. Lett*., **65** [1] (2011) 110–112.
16. Y.S. Hua, W.D. Zhuang, H.Q. Ye, D. Wang, S. Zhang, X. Huang, "A novel red phosphor for white light emitting diodes", *J. Alloys Compd*., **390** [1-2] (2005) 226–229.
17. L.Y. Zhou, J.X. Shi, M.L. Gong, "Red phosphor SrY_2O_4: Eu^{3+} synthesized by the sol-gel method", *J. Lumin*., **113** [3-4] (2005) 285–290.
18. S.S. Yao, Y.Y. Li, L.H. Hue, Y.W. Yan, "Luminescent properties of $Ba_2ZnSi_2O_7$: Eu^{3+} phosphors prepared by sol-gel process", *Eur. Phys. J. Appl. Phys*., **48** (2009) 20602.
19. M. Yu, J. Lin, J. Fang, "Silica spheres coated with YVO_4: Eu^{3+} layers via sol-gel process: A simple method to obtain spherical core-shell phosphors", *Chem. Mater*., **17** [7] (2005) 1783–1791.
20. Y. Kawahara, V. Petrykin, T. Ichihara, N. Kijima, "Synthesis of high-brightness sub-micrometer Y_2O_2S red phosphor powders by complex homogeneous precipitation method", *Chem. Mater*., **18** [26] (2006) 6303–6307.
21. K.N. Kim, H.K. Jung, H.D. Park, D. Kim, "Synthesis and characterization of red phosphor (Y,Gd)BO_3: Eu by the co-precipitation method", *J. Mater. Res*., **17** [4] (2002) 907–910.
22. L.S. Wang, Y.H. Zhou, Z.W. Quan, J. Lin, "Formation mechanisms and morphology dependent luminescence properties of Y_2O_3: Eu phosphors prepared by spray pyrolysis process", *Mater. Lett*., **59** [10] (2005) 1130–1133.
23. Y.C. Kang, S.B. Park, W. Lenggoro,, "Preparation of nonaggregated Y_2O_3: Eu phosphor particles by spray pyrolysis method", *J. Mater. Res*., **14** [6] (1999) 2611–2615.
24. K.H. Kim, J.K. Park, C.H. Kim, H.D. Park, "Synthesis of $SrTiO_3$: Pr, Al by ultrasonic spray pyrolysis", *Ceram. Int*., **28** [1] (2002) 29–36.
25. D.S. Kim, R.Y. Lee, "Synthesis and photoluminescence properties of (Y,Gd)BO_3: Eu phosphor prepared by ultrasonic spray", *J. Mater. Sci*., **35** [19] (2000) 4777–4782.
26. J. Yang, Z.W. Quan, D.Y. Kong, X.M. Liu, "Y_2O_3: Eu^{3+} microspheres: Solvothermal synthesis and luminescence properties", *Cryst. Growth. Des*., **7** [4] (2007) 730–735.
27. G. Jia, Y.H. Song, M. Yang, Y. Huang, L. Zhang, H. You, "Uniform YVO_4: Ln^{3+} (Ln = Eu, Dy, and Sm) nanocrystals: Solvothermal synthesis and luminescence properties", *Opt. Mater*., **31** [6] (2009) 1032–1037.
28. F.B. Cao, "Sol-gel synthesis of red-emitting phosphor Ca-Sr-Mo-W-O-(Eu^{3+},La^{3+}) powders and luminescence properties", *Ind. Eng. Chem. Res*., **51** [9] (2012) 3569–3574.
29. S.X. Yan, J.H. Zhang, X. Zhang, S. Lu, "Enhanced red emission in $CaMoO_4$: Bi^{3+},Eu^{3+}", *J. Phys. Chem. C*, **111** [35] (2007) 13256–13260.
30. Q.L. Dai, *Luminescence Properties of Rare Earth Activated Tungstate and Sulfur Oxide Nanocrystals*, Changchun Inst. Optics, Fine Mech. Phys., Chinese Academy of Sciences, Changchun, 2009.
31. F.Q. Ren, D.H. Chen, "A novel red-emitting phosphor for white light-emitting diodes", *J. Alloys Compd*., **499** [1] (2010) 53–56.
32. S.Y. Hyoung, S.J. Ho, B.I. Won, H.K. Jong, "Particle size control of a monodisperse spherical Y_2O_3: Eu^{3+} phosphor and its photoluminescence properties", *J. Mater. Res*., **22** [1] (2007) 2017–2024.
33. F.A. Rabuffetti, J.S. Lee, R.L. Brutchey, "Vapor diffusion sol-gel synthesis of fluorescent perovskite oxide nanocrystals", *Adv. Mater*., **24** [4] (2012) 1434–1438.
34. J.L. Huang, L.Y. Zhou, Q. Pang, F. Gong, "Photoluminescence properties of a novel phosphor CaB_2O_4: Eu^{3+} under NUV excitation", *Luminescence*, **24** [6] (2009) 363–366.
35. Q.S. Lu, Z.Y. Wang, P.Y. Wang, J. Li, "Structure and luminescence properties of Eu^{3+}-doped cubic mesoporous silica thin films", *Nanoscale Res. Lett*., **5** [11] (2010) 761–768.
36. Z.L. Wang, H.B. Liang, M.L. Gong, Q. Su, "Novel red phosphor of Bi^{3+}, Sm^{3+} co-activated $NaEu(MoO_4)_2$", *Opt. Mater*., **29** [7] (2007) 896–900.

37. Y. Zhai, S. Feng, Z. Zhang, L.J. Shi, X.H. Hao,, "Synthesis and properties of a new red phosphor $SrMgSi_2O_6$: Eu^{3+},M (M = Gd^{3+}, Ti^{4+}) for white LED and its properties", *Rare Metal. Mater. Eng*., **39** [10] (2010) 1825–1828.
38. Z.P. Yang, Y.C. Song, Y. Han, Q. Zhao, F. Pan, D.Z. Zhou, "Preparation and luminescence properties of novel red phosphor Sr_2ZnMoO_6: Sm^{3+} phosphor", *Chin. J. Lumin*., **33** [6] (2012) 586–590.
39. J. Sun, J. Lai, H. Du, "Synthesis and luminescence properties of red emitting phosphors $Na_3CaB_5O_{10}$: Eu^{3+}", *Adv. Mater. Res*., **295-297** [543] (2011) 547–550.
40. A. Gangadharan, M. Pokhrel, M. Alejandrina Martínez Gámez, D.K. Sada, "Synthesis and upconversion spectroscopy of Yb, Er doped M_2O_2S (M = La, Gd, Y) phosphors", *Sci. Adv. Mater*., **4** [5-6] (2012) 623–630.
41. Y.C. Chang, Y.S. Chang, "Synthesis and photoluminescence characteristics of color-tunable BaY_2ZnO_5: Eu^{3+} phosphors", *Appl. Phys. Lett*., **93** [21] (2008) 2–3.